# High-Throughput Analysis of Concentration-Dependent Antibody Self-Association

Shantanu V. Sule,[†] Muppalla Sukumar,[‡*] William F. Weiss, IV,[‡] Anna Marie Marcelino-Cruz,[†] Tyler Sample,[†] and Peter M. Tessier[†*]

[†]Center for Biotechnology and Interdisciplinary Studies, and Department of Chemical and Biological Engineering, Rensselaer Polytechnic Institute, Troy, New York; and [‡]Biopharmaceutical Research and Development, Lilly Research Laboratories, Eli Lilly and Company, Indianapolis, Indiana

ABSTRACT Monoclonal antibodies are typically monomeric and nonviscous at low concentrations, yet they display highly variable associative and viscous behavior at elevated concentrations. Although measurements of antibody self-association are critical for understanding this complex behavior, traditional biophysical methods are not capable of characterizing such concentration-dependent self-association in a high-throughput manner. Here we describe a nanoparticle-based method, termed self-interaction nanoparticle spectroscopy, that is capable of rapidly measuring concentration-dependent self-interactions for three human monoclonal antibodies with unique solution behaviors. We demonstrate that gold nanoparticles conjugated with antibodies at low protein concentrations (<40 $\mu$g/mL) display self-association behavior (as measured by the interparticle distance-dependent plasmon wavelength) that is well correlated with static light-scattering measurements obtained at three orders of magnitude higher antibody concentrations. Using this methodology, we find that the antibodies display a complex pH-dependent self-association behavior that is strongly influenced by the solution ionic strength. Importantly, we find that a polyclonal human antibody is nonassociative for all solution conditions evaluated in this work, suggesting that antibody self-association is more specific than previously realized. We expect that our findings will guide rational manipulation of antibody phase behavior, and enable studies that elucidate sequence and structural determinants of antibody self-association.

## INTRODUCTION

One of the most fundamental properties of proteins is their propensity to self-associate. In some cases, protein self-association is linked to normal biological function (e.g., assembly of microtubules and actin filaments) (1,2). In other cases, proteins inappropriately self-associate and aggregate, leading to several human disorders (e.g., Alzheimer's and prion diseases) (3,4) and the inactivation of therapeutic proteins (e.g., antibodies) (5–9). Given the deleterious nature of protein aggregation, it is critical to elucidate the underlying protein self-interactions so that we can develop systematic strategies to prevent this undesirable behavior.

Monoclonal antibodies (mAbs) are an important class of therapeutic proteins that display highly complex and poorly understood self-association behavior (10–13). These large, multidomain proteins possess two identical antigen-binding domains (Fabs) that can participate in homotypic interactions with themselves and heterotypic interactions with their constant (Fc) domains (11). Given the high sequence similarity between mAb variants, it would be logical to assume that mAbs display similar self-association and solubility behavior. However, the highly variable complementarity determining regions (CDRs) on the surface of Fabs contribute disproportionately to mAb self-association (11,14,15), as single point mutations within CDRs can dramatically impact the solution properties of mAbs and antibody fragments (14–16).

The self-association behavior of mAbs is highly concentration-dependent (5,17). Generally, mAbs are well behaved at low protein concentrations (<10 mg/mL) and display a modest propensity to self-associate. However, at the high concentrations required for therapeutic applications (>50 mg/mL), mAbs display highly variable self-association behavior that is difficult to predict based on antibody sequence or structure ((18,19) for recent progress). Such associative behavior can lead to viscous, opalescent, and/or aggregated antibody solutions (6,20). Antibodies (and other proteins) self-associate at high concentrations via interactions sampled both frequently (e.g., Coulombic interactions) and infrequently (e.g, induced dipole interactions) at low concentrations (17,21).

Therefore, it is critical to measure the self-association behavior of mAbs at high concentrations to understand their complex phase behavior (22–25). This ambitious goal is difficult to achieve in practice because many analytical methods that are capable of measuring protein self-interactions in dilute solutions (26–28) are not amenable to measuring such interactions in highly concentrated solutions, especially in a high-throughput manner (14,29,30). A second limitation is that a large amount of antibody is required to analyze high-concentration self-association behavior, which restricts analysis of these complex interactions.

*Submitted May 12, 2011, and accepted for publication August 22, 2011.*

*Correspondence: tessier@rpi.edu or sukumar_muppalla@lilly.com

Editor: Jason M. Haugh.



0006-3495/11/10/1749/9 $2.00

doi: 10.1016/j.bpj.2011.08.036

We seek to address both limitations by using a nanoparticle-based assay, termed self-interaction nanoparticle spectroscopy (SINS), to measure protein self-interactions (31,32). We reason that 1) antibodies at low concentrations (<40 $\mu$g/mL) can be adsorbed on gold nanoparticles to generate antibody clusters in which the local protein concentration is extremely high (>100 mg/mL); and 2) the interparticle distances between the polyvalent antibody-gold conjugates can be determined by multibody interactions that occur in concentrated antibody solutions.

This approach builds on our previous high-throughput analysis of globular protein self-association (31,32), but is distinct in that it seeks to evaluate high-concentration self-association behavior for large, multidomain proteins. Our choice of gold nanoparticles is based on several factors, including the excellent stability and functionality of antibodies adsorbed on gold particles (33,34), as evidenced by decades of use of these conjugates in immunohistochemistry studies (35,36). We also chose to use gold particles because of their interparticle distance-dependent optical properties (37–39). The plasmon wavelength ($\lambda_p$), i.e., the wavelength corresponding to maximal absorbance of gold colloid, shifts to greater values as the separation distance between nanoparticles is reduced. We seek to exploit the sensitivity of the plasmon wavelength to changes in the interparticle distances between antibody-gold conjugates to quantify the extent of antibody self-association. Herein, we demonstrate that SINS is well suited to characterize the concentration-dependent self-association behavior of multiple mAbs, and we employ this methodology to elucidate complex antibody self-association behavior that is strongly dependent on solution pH and ionic strength.

## MATERIALS AND METHODS

### Materials

Three human Ig4 mAbs (expressed in CHO cells) were provided by Eli Lilly and Company (Indianapolis, IN). Gold nanoparticles (20 nm) were obtained from Ted Pella (15705-1; Redding, CA). Traut's reagent (PI-26101), Ellman's reagent (PI-22582), potassium chloride (BP366-500), potassium hydroxide (ACS grade, P250), glacial acetic acid (99.5% pure; 124040010), recombinant Protein A (PI-21184), and a MicroBCA assay kit (PI-23235) were obtained from Thermo Fisher Scientific (Waltham, MA). Citric acid (ACS grade, 251275), sodium citrate (USP grade, S1804), dibasic sodium phosphate dihydrate (ACS grade, 71643), monobasic potassium phosphate (ACS grade, P0662), potassium acetate (P1190), hydrochloric acid (37% ACS grade, 320331), bovine serum albumin (A2153), polyclonal IgG from human serum (I4506), and mercaptopolyethylene glycol monomethyl ether (5000 MW, 11124) were purchased from Sigma-Aldrich (St. Louis, MO). Sodium chloride (102892) was obtained from MP Biomedicals (Solon, OH). All experiments were carried out at room temperature (23 ± 2°C). Antibody concentrations were determined via absorption measurements (280 nm) using extinction coefficients of 1.46 (mAb1), 1.47 (mAb2), and 1.61 (mAb3) mL/(mg·cm). The extinction coefficients were calculated using an adaptation of the Edelhoch method (40), and verified experimentally using amino acid analysis.

### Antibody immobilization

Each antibody (30 $\mu$M) that was thiolated before immobilization was modified with Traut's reagent (180 $\mu$M) for 1 h (pH 8.0, PBS, 2 mM EDTA, 23°C). The modified antibodies were then buffer exchanged (Zeba desalting columns; Thermo Fisher Scientific) into acetate buffer (20 mM potassium acetate, pH 4.3). The extent of thiolation was quantified by means of Ellman's assay. One part of wild-type or thiolated antibody solution (400 $\mu$g/mL) was mixed with nine parts of gold particles ($4.7 \times 10^{12}$ particles/mL) and incubated overnight at 23°C. The next day, the conjugates were pelleted (15,000 rpm for 10 min), the supernatant (90% of starting volume) was discarded, and the conjugates were resuspended in immobilization buffer (2 mM potassium acetate, pH 4.3) supplemented with thiolated PEG (5000 MW; 0.1 $\mu$M). After 1 h, the conjugates were pelleted and resuspended in immobilization buffer.

### Dynamic light scattering

Dynamic light scattering (DLS) analysis was conducted using a DynaPro Titan light-scattering setup (Wyatt, Santa Barbara, CA). Gold particles and antibodies were filtered separately with a 0.22 $\mu$m PVDF filter and then combined as described above. The conjugates were transferred into disposable Eppendorf light-scattering cuvettes without further processing. Antibody samples (0.5 mg/mL) in immobilization buffer were filtered directly into the light-scattering cuvette. For solutions containing nanoparticles, the laser power was adjusted accordingly to maintain a count rate of 1–2 million counts per second. For antibody solutions without nanoparticles, the laser power was adjusted to obtain hundreds of thousands of counts per second. The scattering data were fit (Dynamics software; Wyatt) assuming the scatterers to be Rayleigh spheres.

### Plasmon wavelength measurements

The purified antibody-gold conjugates were added to various buffered stock solutions in a volumetric ratio of 4:1, respectively, in clear 96-well microtiter plates. The resulting pH of these solutions was adjusted to 4.3 or 6/6.5, and the final buffer concentrations were 20 mM acetate (pH 4.3) and 10 mM citrate (pH 6/6.5). The absorption spectra (400–700 nm) of each sample (175 $\mu$L) were measured with a Tecan Safire$^2$ plate reader. We identified the plasmon wavelength by fitting the absorption spectra to a quadratic polynomial (40 data points, intervals of 1 nm) and evaluating the wavelength at which the first derivative of the quadratic function was zero.

### Antibody adsorption analysis

Antibodies at varying concentrations (5–40 $\mu$g/mL) were adsorbed on gold particles overnight (9:1 volumetric ratio of gold/antibody, 1 mL total volume). The next day, the conjugates were pelleted and resuspended twice (90% of supernatant removed and replaced each time). The conjugates were then resuspended in microBCA assay solution (Thermo Fisher Scientific), developed for 2 h at 32°C, the absorbance was measured at 562 nm, and the adsorbed concentration was calculated using a standard curve developed with the same antibodies.

### Static light scattering

Weight average molecular weight (WAMW) values were determined for each antibody (6 and 42 mg/mL) in different buffer systems using static light scattering (SLS). Measurements were performed at room temperature (23 ± 2°C) with the use of an LSE-5003 multiple tau digital correlator and CGS-3 compact goniometer system (ALV, Langen, Germany). Samples were dialyzed against excess buffer, and final antibody concentrations

were determined with an Agilant 8453 UV-visible spectrophotometer (Agilent Technologies, Santa Clara, CA). Samples were filtered through 0.22-$\mu$m, 13-mm Millex GV durapore membrane filters (Millipore, Billerica, MA) immediately before measurement. The intensities at multiple angles (70–110°) were averaged because scattering was independent of the scattering angle. The WAMW values were calculated as follows:

$$\mathrm{WAMW} = \left(\frac{Kc}{R_{ex}}\right)^{-1}, \quad (1)$$

where $K$ is an optical constant, $c$ is the protein mass concentration, and $R_{ex}$ is the excess Rayleigh ratio (41). The value of the refractive index increment (d$n$/d$c$) used to calculate $K$ was 0.185 mL/g.

### Protein A binding analysis

Protein A from *Staphylococcus aureus* (45 kDa; Pierce) prepared at 80 and 160 $\mu$g/mL (PBS, pH 7) was mixed with antibody-gold conjugates (20-fold concentrated, free antibody removed) in immobilization buffer in a 1:1 volumetric ratio, and incubated for 90 min. Afterward, the samples were centrifuged for 10 min (15,000 rpm), and the concentration of Protein A remaining in the supernatant was assayed using the microBCA assay (Pierce). The amount of bound Protein A was calculated as the difference between the initial and final amounts of Protein A in solution, and BSA-gold conjugates were used to account for nonspecifically bound Protein A. Separately, equal volumes of Protein A (80 and 160 $\mu$g/mL in PBS at pH 7) and unconjugated mAbs (in immobilization buffer) were mixed for 90 min. Afterward, the Protein A-mAb solutions were spin-filtered (50 kDa molecular mass cutoff filters; Millipore) for 20 min (12,000 rpm) to separate bound and unbound Protein A. We determined the filtrate concentration of unbound Protein A using the microBCA assay, and calculated the amount of bound Protein A via mass balance. Protein A solutions without antibody were also filtered to account for nonspecific protein retention.

## RESULTS

### Assembly and characterization of gold-antibody conjugates

Toward our goal of using antibody-gold conjugates to characterize antibody self-association, we first sought to immobilize two mAbs (mAb1 and mAb2) on gold nanoparticles (20 nm) in a manner that would result in a near-monolayer coverage. We tested two approaches for immobilizing antibodies: one in which the wild-type antibody is directly adsorbed, and the other in which primary amines on the antibody surface are converted to thiol moieties to facilitate immobilization. We used Traut's reagent to convert approximately one primary amine per antibody to a thiol moiety, and confirmed this modification using Ellman's reagent. Next, we investigated a range of pH and ionic strength values to identify conditions that would lead to antibody immobilization for both wild-type and thiolated antibodies while promoting high colloidal stability of the conjugates. To that end, we first measured the visible spectra of mAb1 and mAb2 conjugates to evaluate solution conditions that would promote plasmon shifts of ~1% relative to nonconjugated gold particles, characteristic of changes in the dielectric environment surrounding nanoparticles due to protein adsorption (42,43). We found that moderately acidic pH (4.3) in the absence of salt led to such plasmon shifts (6–7 nm) for both wild-type and thiolated antibodies (Fig. 1 *A* and Fig. S1 in the Supporting Material), consistent with antibody adsorption without association between conjugates. In contrast, we were unable to identify such solution conditions at higher (pH 6–7) and/or ionic strength (50–300 mM; data not shown). We also found that wild-type and thiolated antibodies display indistinguishable plasmon shifts upon antibody adsorption at pH 4.3 (Fig. 1 *A* and Fig. S1).

We also used DLS to characterize the size of mAb1 and mAb2 conjugates (Fig. 1 *B*). The measured radius of the gold colloid (9.3 ± 1.1 nm) is close to its nominal value (10 nm). Moreover, the radii of both wild-type and thiolated antibodies (4.7–5.4 nm) are close to each other and consistent with previous reports (44,45). The radii of the gold-antibody conjugates (19–23 nm) for wild-type and thiolated antibodies are similar and consistent with a monolayer coverage of antibody (19–21 nm). Nevertheless, we also quantified the amount of immobilized protein for both

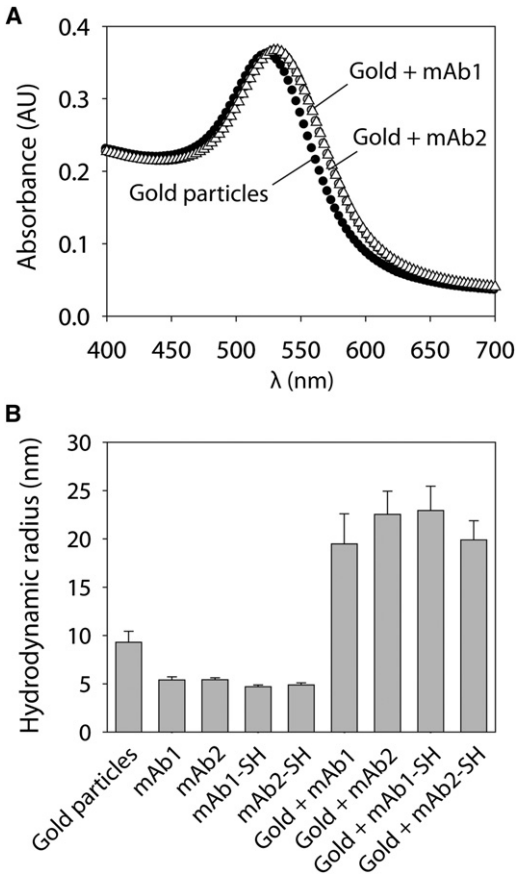


FIGURE 1 Immobilization of mAbs on gold nanoparticles. (*A*) UV-visible absorbance spectra of gold particles (*black circles*), gold-mAb1 conjugates (*gray circles*), and gold-mAb2 conjugates (*white triangles*). (*B*) DLS analysis of gold particles, antibodies (wild-type and thiolated), and gold-antibody conjugates.

wild-type and thiolated antibodies (Fig. S2), and found immobilization densities (3.0–4.1 mg/m$^2$ or 13–17 antibodies/particle) that are similar to literature values (1–5 mg/m$^2$) (42,43,46,47) and theoretical values for a monolayer surface coverage (2–5 mg/m$^2$) (46) that vary based on the orientation of the adsorbed antibody. We conclude that thiolation is unnecessary for antibody immobilization, and thus we further investigate only wild-type antibodies conjugated to gold colloid.

We also evaluated whether the immobilized antibodies are randomly oriented on the gold surface. To accomplish this, we investigated binding of Protein A to the conjugated mAbs. We hypothesized that randomly oriented antibodies would retain half of their Protein A binding activity because half of the binding sites would be blocked by the gold surface. We found that both mAb1- and mAb2-gold conjugates retain approximately half of their Protein A binding activity (52% for mAb1 and 53% for mAb2) relative to unconjugated mAbs (Fig. S3). Our findings suggest that mAb1 and mAb2 are immobilized in a near-random distribution of antibody orientations.

## Comparison of SINS and light-scattering measurements

We next investigated the self-association behavior of both mAb1 and mAb2 conjugates at near-neutral pH (6–6.5). We find that the plasmon wavelengths for mAb2 conjugates assembled at pH 4.3 ($\lambda_p = 530.7 \pm 0.1$ nm) increase significantly when the solution pH is increased to pH 6 (Fig. 2 *A*; $\lambda_p > 535$ nm). Moreover, the plasmon wavelength for mAb2 conjugates at pH 6 is lower at 150 mM NaCl than at 50 mM NaCl. In contrast, the plasmon wavelengths for mAb1 conjugates at pH 6.5 (Fig. 2 *A*; $\lambda_p = 530.8 \pm 0.1$ nm) are indistinguishable from those at low pH ($\lambda_p = 530.7 \pm 0.1$ nm). We performed SLS measurements of the WAMW (6 mg/mL) for each antibody and solution condition to evaluate whether the SINS measurements are reflective of antibody self-association in the absence of nanoparticles (Fig. 2 *B*). We expected that attractive antibody self-interactions (as indicated by increased values of WAMW) would correspond to decreased separation distances between antibody-gold conjugates (as indicated by increased plasmon wavelengths). We found that large WAMW values correspond to large plasmon wavelengths (Fig. 2).

Nevertheless, we sought to more rigorously evaluate the relationship between the SINS and light-scattering measurements over a wider range of ionic strengths (Fig. 3). Relative to noninteracting gold-antibody conjugates, we find that mAb1 is nonassociative at pH 6.5 (0–300 mM NaCl) but does associate at pH 4.3 at sodium chloride concentrations $\geq$25 mM (Fig. 3 *A*). In contrast, mAb2 is highly associative at near-neutral pH (pH 6; 0–300 mM NaCl) and weakly associative at pH 4.3 (Fig. 3 *B*). We confirmed that the amount of immobilized antibody was similar for conjugates

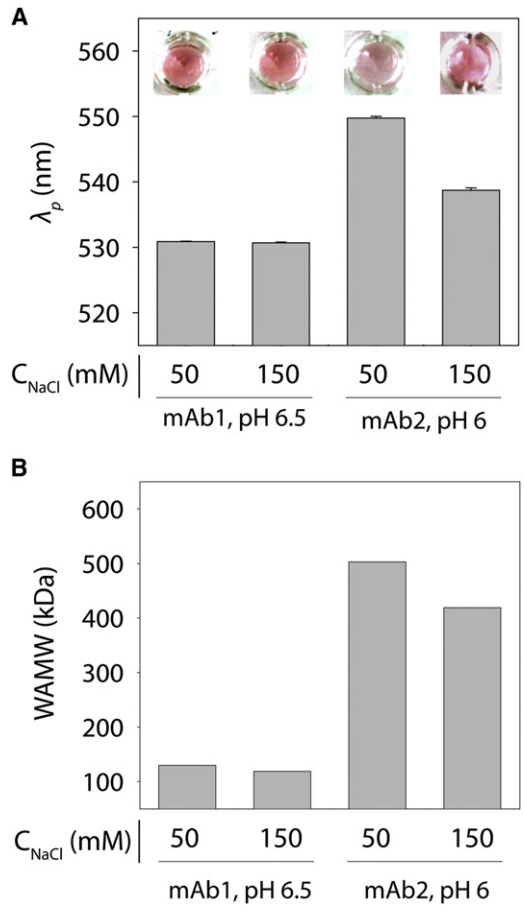


FIGURE 2 Analysis of variable antibody self-association at near-neutral pH. (*A*) Plasmon wavelengths ($\lambda_p$) of mAb1 and mAb2 conjugates at pH 6.5 and 6, respectively. (*B*) SLS measurements of WAMW values for mAb1 and mAb2 at 6 mg/mL.

in different solution conditions (Fig. S4), and that the buffer type weakly affected the SINS measurements (Fig. S5). Of importance, the light-scattering measurements (6 mg/mL) are consistent with our plasmon wavelength measurements, because mAb1 is more associative at pH 4.3 than at pH 6.5 (Fig. 4 *A*), and the inverse is true for mAb2 (Fig. 4 *B*).

To provide a more quantitative comparison between our SINS and light-scattering results, we plotted the plasmon wavelengths for mAb1 and mAb2 (32 $\mu$g/mL) against WAMW values (normalized to the approximate monomer molecular mass of 150 kDa) measured at low (6 mg/mL) and high (42 mg/mL) antibody concentrations (Fig. 5). In both cases, we find that plasmon wavelengths are well correlated with normalized WAMW values ($R^2 = 0.89$–$0.97$). We also observe a better correlation between plasmon wavelengths and WAMW values measured at higher antibody concentrations ($R^2 = 0.97$) compared with those obtained at lower concentrations ($R^2 = 0.89$).

To evaluate the robustness of SINS to measure self-association of other mAbs, we characterized a third antibody (mAb3). We performed SLS analysis of mAb3 at

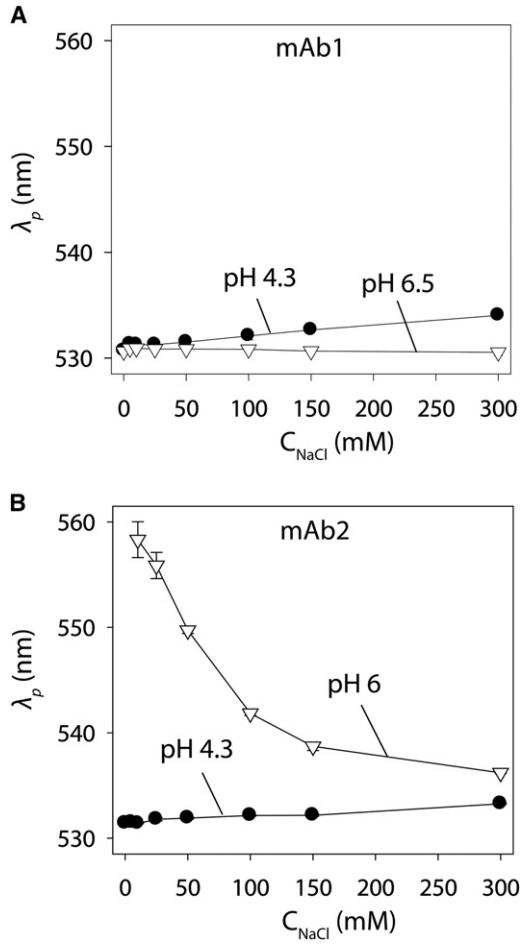


FIGURE 3 SINS analysis of antibody self-association as a function of pH and ionic strength. Plasmon wavelengths ($\lambda_p$) of (*A*) gold-mAb1 and (*B*) gold-mAb2 conjugates at pH 4.3 (*solid circles*) and pH 6.5/6 (*open triangles*).

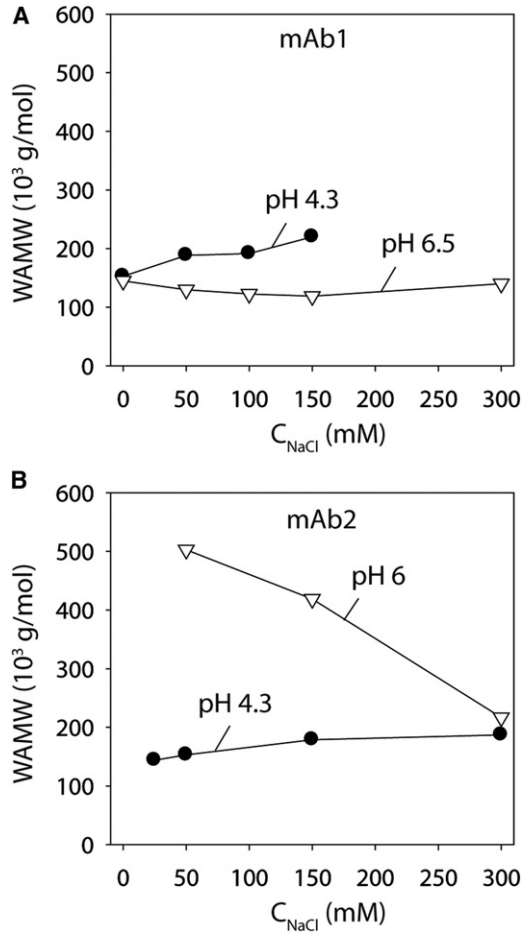


FIGURE 4 SLS analysis of antibody self-association as a function of pH and ionic strength. WAMW measurements for (*A*) mAb1 and (*B*) mAb2 (6 mg/mL) at pH 4.3 (*solid circles*) and pH 6.5 (*open triangles*).

pH 6.5, and found that it is more associative than mAb1 but less associative than mAb2 (Fig. 6 *A* and Fig. S6). To evaluate mAb3 self-association using SINS, we first characterized the size and immobilization density of mAb3-gold conjugates. We found that the mAb3 conjugates are similar in size (18.5 ± 1.5 nm; Fig. S6) and antibody loading (2.5 ± 0.1 mg/m$^2$) to the mAb1 and mAb2 conjugates (Fig. 1 *B* and Fig. S2). The plasmon wavelengths for mAb3 conjugates are intermediate to those for mAb1 and mAb2, in agreement with the light-scattering results (Fig. 6 *B* and Fig. S6).

### Specificity of SINS measurements

To evaluate the specificity of mAb self-interaction measurements, we sought to determine whether a polyclonal IgG would show unique self-association behavior relative to the mAbs. We hypothesized that the molecular diversity of a polyclonal mixture of antibodies would render it less associative than the mAbs. To test this hypothesis, we first prepared polyclonal antibody-gold conjugates in the same manner employed for each mAb. We found that the immobilization density (3.8 ± 0.6 mg/m$^2$) and size of the conjugates (18.6 ± 0.6 nm; Fig. S7) were consistent with those of their monoclonal counterparts (Fig. 1 *B*, Fig. S2, and Fig. S6). Next, we evaluated the self-association behavior of the polyclonal antibody conjugates at the same pH and ionic strength values analyzed for each mAb (Fig. 7). We found that the polyclonal antibody was nonassociative at all solution conditions examined, revealing that mAbs are significantly more associative than the nonspecific antibody mixture.

## DISCUSSION

A major outcome of this work is our demonstration that SINS measurements of antibody self-interactions at low concentrations (<40 $\mu$g/mL) are well correlated with those obtained by light scattering at three orders of magnitude higher antibody concentrations. We demonstrate that polyvalent antibody-gold conjugates can be used to evaluate

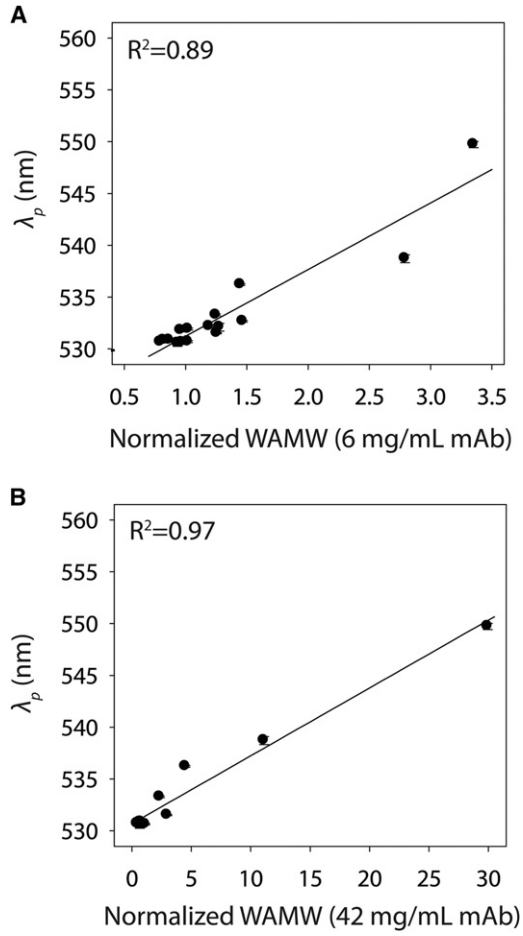


FIGURE 5 Correlation between SINS and SLS measurements of antibody self-association. Plasmon wavelengths ($\lambda_p$) for gold-antibody conjugates plotted versus WAMW values obtained at antibody concentrations of (*A*) 6 and (*B*) 42 mg/mL.

multibody interactions that occur at elevated antibody concentrations. Importantly, our SINS measurements are better correlated with high-concentration (42 mg/mL) light-scattering measurements than with low-concentration (6 mg/mL) measurements. This finding is consistent with our hypothesis that SINS can enable analysis of high-concentration antibody self-association due to the polyvalent display of antibodies on gold particles.

The simplicity of using SINS to measure concentration-dependent antibody self-association in a parallel, high-throughput manner is another important outcome of our work. We conducted our measurements in 96-well microtiter plates with a standard absorbance plate reader. Currently, we require ~15 min and 400 $\mu$g of antibody to measure plasmon wavelengths for 100 samples. We conservatively estimate that the time and amount of antibody could be reduced to 5 min and 100 $\mu$g per 100 samples by reducing the antibody concentration, the number of points collected for each visible absorption spectrum, and the sample volume using 384-well plates.

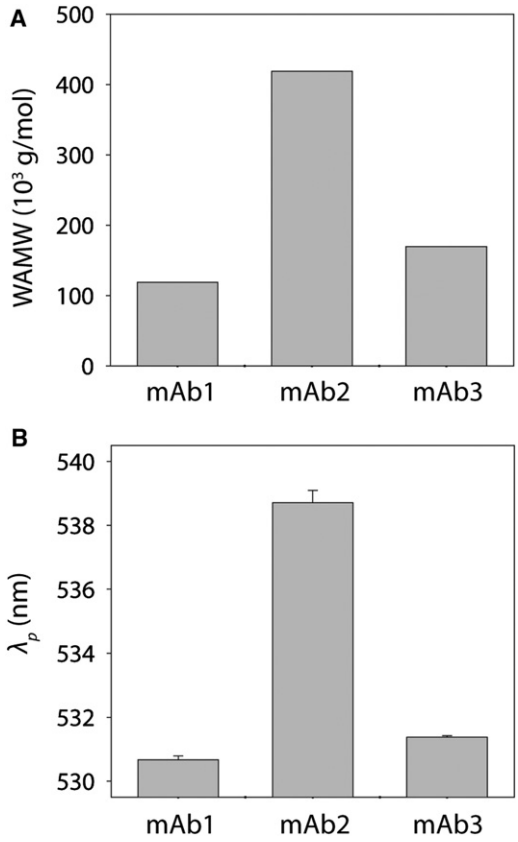


FIGURE 6 Comparison of self-association behavior for three mAbs. Measurements of (*A*) WAMW (6 mg/mL) and (*B*) plasmon wavelengths ($\lambda_p$) at pH 6.5 (mAb1 and mAb3) and pH 6 (mAb2). The salt concentration was 150 mM NaCl.

We investigated multiple methods of immobilizing antibodies on nanoparticles to evaluate whether chemical modification of antibodies is necessary for preparing stable antibody-gold conjugates for SINS analysis. We found

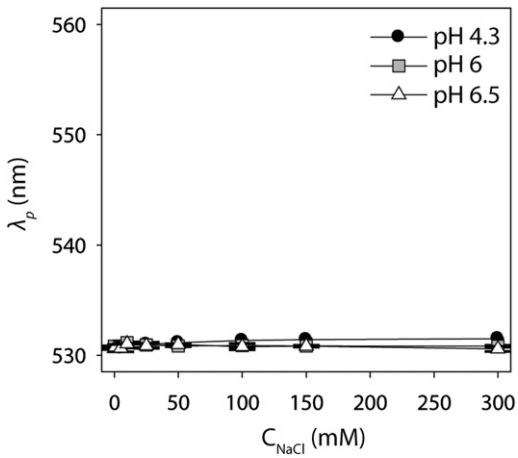


FIGURE 7 Self-association behavior of a polyclonal antibody as a function of pH and ionic strength. Plasmon wavelengths ($\lambda_p$) of polyclonal antibody-gold conjugates at pH 4.3 (*black circles*), pH 6 (*gray squares*) and pH 6.5 (*white triangles*).

that all antibodies studied in this work adsorbed well on gold regardless of whether they were thiolated. All of the unmodified antibodies lacked free thiol groups, confirming that residues other than cysteine mediate adsorption (48–51). Our finding that wild-type antibodies are well adsorbed on gold particles is consistent with much previous work demonstrating that stable antibody-gold conjugates can be generated by simple noncovalent adsorption (35,52,53).

We also made two particularly important methodological advances in performing SINS in this work that deserve further consideration. First, we identified solution conditions (pH 4.3, 2 mM acetate) for antibody immobilization in which antibody-gold conjugates do not associate. This mildly acidic pH and low ionic strength condition enabled us to pellet the antibody-gold conjugates multiple times to remove free protein without causing the conjugates to aggregate. Second, we adsorbed thiolated PEG on the antibody-gold conjugates to reduce nonspecific interactions. Although thiolated PEG does not displace bound antibody (Fig. S2), it significantly improves the correlation between SINS and light-scattering measurements (Fig. 4 *B* and Fig. S8).

The efficiency of SINS enabled us to identify complex pH-dependent patterns of self-association for mAb1 and mAb2. Both antibodies are associative at low pH (4.3) and salt concentrations >25 mM NaCl, consistent with previous reports for other mAbs (54,55). At near-neutral pH (6–6.5), mAb2 is much more associative than mAb1. This solution behavior appears to involve electrostatic interactions, because the association is attenuated with salt (14,56). The striking difference between solution conditions that minimize self-association for mAb1 and mAb2 highlights the complexity of antibody self-association, and the need to measure these interactions to manipulate antibody solution properties in a rational manner.

In contrast to the mAbs, the lack of self-association for the polyclonal antibody over a wide range of solution conditions is striking and suggests that mAb self-association is more specific than is generally expected. Our findings are supported by previous work demonstrating that viscosity measurements of concentrated polyclonal antibody solutions are well described by hard sphere models (which consider only excluded volume contributions to intermolecular interactions) (57), unlike several mAbs that are poorly described by such models (11,23). A potential explanation for this behavior is that the polyclonal nature of this antibody mixture prevents attractive intermolecular interactions (57). Neal and co-workers (58) demonstrated that a small number of pairwise configurations with a high level of geometric complementarity (e.g., the crystal contacts) dominate the overall strength of globular protein self-association. Based on the importance of self-complementarity in protein self-association, we posit that polyclonal antibodies are incapable of forming such complementary pairwise configurations and therefore fail to associate. This hypothesis awaits computational and further experimental verification.

## CONCLUSIONS

In summary, we have demonstrated a high-throughput method for measuring the concentration-dependent self-association of mAbs at low protein concentrations. We believe that clustering antibodies and other proteins around nanometer-sized particles is an important approach for understanding high-concentration solution behavior. It is likely that variations in nanoparticle size and composition, as well as in protein immobilization density and chemistry, will lead to additional advances in SINS characterization of antibody self-interactions at low and high protein concentrations. We expect that implementing SINS and related methods to characterize the self-association behavior of homologous libraries of antibodies will reveal key sequence and structural determinants of concentration-dependent antibody self-association.

## SUPPORTING MATERIAL

Eight figures are available at http://www.biophysj.org/biophysj/supplemental/S0006-3495(11)01009-5.

We thank Mark Pollo for performing SLS measurements.

This work was supported by Eli Lilly.

## REFERENCES

1. Voter, W. A., and H. P. Erickson. 1984. The kinetics of microtubule assembly. Evidence for a two-stage nucleation mechanism. *J. Biol. Chem.* 259:10430–10438.
2. Pollard, T. D., and G. G. Borisy. 2003. Cellular motility driven by assembly and disassembly of actin filaments. *Cell.* 112:453–465.
3. Chiti, F., and C. M. Dobson. 2006. Protein misfolding, functional amyloid, and human disease. *Annu. Rev. Biochem.* 75:333–366.
4. Tessier, P. M., and S. Lindquist. 2009. Unraveling infectious structures, strain variants and species barriers for the yeast prion [PSI+]. *Nat. Struct. Mol. Biol.* 16:598–605 (PSI+).
5. Shire, S. J., Z. Shahrokh, and J. Liu. 2004. Challenges in the development of high protein concentration formulations. *J. Pharm. Sci.* 93:1390–1402.
6. Manning, M. C., D. K. Chou, …, D. S. Katayama. 2010. Stability of protein pharmaceuticals: an update. *Pharm. Res.* 27:544–575.
7. Daugherty, A. L., and R. J. Mrsny. 2006. Formulation and delivery issues for monoclonal antibody therapeutics. *Adv. Drug Deliv. Rev.* 58:686–706.
8. Chi, E. Y., S. Krishnan, …, J. F. Carpenter. 2003. Physical stability of proteins in aqueous solution: mechanism and driving forces in nonnative protein aggregation. *Pharm. Res.* 20:1325–1336.
9. Weiss, 4th, W. F., T. M. Young, and C. J. Roberts. 2009. Principles, approaches, and challenges for predicting protein aggregation rates and shelf life. *J. Pharm. Sci.* 98:1246–1277.
10. Ahamed, T., B. N. Esteban, …, J. Thömmes. 2007. Phase behavior of an intact monoclonal antibody. *Biophys. J.* 93:610–619.
11. Kanai, S., J. Liu, …, S. J. Shire. 2008. Reversible self-association of a concentrated monoclonal antibody solution mediated by Fab-Fab

interaction that impacts solution viscosity. *J. Pharm. Sci.* 97:4219–4227.

12. Wang, W., S. Singh, …, S. Nema. 2007. Antibody structure, instability, and formulation. *J. Pharm. Sci.* 96:1–26.
13. Gibson, T. J., K. Mccarty, …, D. B. Volkin. 2011. Application of a high-throughput screening procedure with PEG-induced precipitation to compare relative protein solubility during formulation development with IgG1 monoclonal antibodies. *J. Pharm. Sci.* 100:1009–1021.
14. Scherer, T. M., J. Liu, …, A. P. Minton. 2010. Intermolecular interactions of IgG1 monoclonal antibodies at high concentrations characterized by light scattering. *J. Phys. Chem. B.* 114:12948–12957.
15. Wu, S. J., J. Luo, …, Y. Feng. 2010. Structure-based engineering of a monoclonal antibody for improved solubility. *Protein Eng. Des. Sel.* 23:643–651.
16. Perchiacca, J. M., M. Bhattacharya, and P. M. Tessier. 2011. Mutational analysis of domain antibodies reveals aggregation hotspots within and near the complementarity determining regions. *Proteins.* 79:2637–2647.
17. Liu, J., M. D. Nguyen, …, S. J. Shire. 2005. Reversible self-association increases the viscosity of a concentrated monoclonal antibody in aqueous solution. *J. Pharm. Sci.* 94:1928–1940.
18. Chennamsetty, N., B. Helk, …, B. L. Trout. 2009. Aggregation-prone motifs in human immunoglobulin G. *J. Mol. Biol.* 391:404–413.
19. Chennamsetty, N., V. Voynov, …, B. L. Trout. 2009. Design of therapeutic proteins with enhanced stability. *Proc. Natl. Acad. Sci. USA.* 106:11937–11942.
20. Mahler, H. C., W. Friess, …, S. Kiese. 2009. Protein aggregation: pathways, induction factors and analysis. *J. Pharm. Sci.* 98:2909–2934.
21. Yadav, S., J. Liu, …, D. S. Kalonia. 2010. Specific interactions in high concentration antibody solutions resulting in high viscosity. *J. Pharm. Sci.* 99:1152–1168.
22. Harn, N., C. Allan, …, C. R. Middaugh. 2007. Highly concentrated monoclonal antibody solutions: direct analysis of physical structure and thermal stability. *J. Pharm. Sci.* 96:532–546.
23. Salinas, B. A., H. A. Sathish, …, T. W. Randolph. 2010. Understanding and modulating opalescence and viscosity in a monoclonal antibody formulation. *J. Pharm. Sci.* 99:82–93.
24. Gabrielson, J. P., M. L. Brader, …, T. W. Randolph. 2007. Quantitation of aggregate levels in a recombinant humanized monoclonal antibody formulation by size-exclusion chromatography, asymmetrical flow field flow fractionation, and sedimentation velocity. *J. Pharm. Sci.* 96:268–279.
25. Saluja, A., R. M. Fesinmeyer, …, Y. R. Gokarn. 2010. Diffusion and sedimentation interaction parameters for measuring the second virial coefficient and their utility as predictors of protein aggregation. *Biophys. J.* 99:2657–2665.
26. Chi, E. Y., S. Krishnan, …, T. W. Randolph. 2003. Roles of conformational stability and colloidal stability in the aggregation of recombinant human granulocyte colony-stimulating factor. *Protein Sci.* 12:903–913.
27. Pekar, A., and M. Sukumar. 2007. Quantitation of aggregates in therapeutic proteins using sedimentation velocity analytical ultracentrifugation: practical considerations that affect precision and accuracy. *Anal. Biochem.* 367:225–237.
28. Curtis, R. A., J. Ulrich, …, H. W. Blanch. 2002. Protein-protein interactions in concentrated electrolyte solutions. *Biotechnol. Bioeng.* 79:367–380.
29. Gabrielson, J. P., T. W. Randolph, …, M. R. Stoner. 2007. Sedimentation velocity analytical ultracentrifugation and SEDFIT/c(s): limits of quantitation for a monoclonal antibody system. *Anal. Biochem.* 361:24–30.
30. Kingsbury, J. S., and T. M. Laue. 2011. Fluorescence-detected sedimentation in dilute and highly concentrated solutions. *Methods Enzymol.* 492:283–304.
31. Tessier, P. M., J. Jinkoji, …, A. M. Lenhoff. 2008. Self-interaction nanoparticle spectroscopy: a nanoparticle-based protein interaction assay. *J. Am. Chem. Soc.* 130:3106–3112.
32. Bengali, A. N., and P. M. Tessier. 2009. Biospecific protein immobilization for rapid analysis of weak protein interactions using self-interaction nanoparticle spectroscopy. *Biotechnol. Bioeng.* 104:240–250.
33. El-Sayed, I. H., X. Huang, and M. A. El-Sayed. 2005. Surface plasmon resonance scattering and absorption of anti-EGFR antibody conjugated gold nanoparticles in cancer diagnostics: applications in oral cancer. *Nano Lett.* 5:829–834.
34. Baptista, P., E. Pereira, …, R. Franco. 2008. Gold nanoparticles for the development of clinical diagnosis methods. *Anal. Bioanal. Chem.* 391:943–950.
35. Geoghegan, W. D., and G. A. Ackerman. 1977. Adsorption of horseradish peroxidase, ovomucoid and anti-immunoglobulin to colloidal gold for the indirect detection of concanavalin A, wheat germ agglutinin and goat anti-human immunoglobulin G on cell surfaces at the electron microscopic level: a new method, theory and application. *J. Histochem. Cytochem.* 25:1187–1200.
36. Copland, J. A., M. Eghtedari, …, A. A. Oraevsky. 2004. Bioconjugated gold nanoparticles as a molecular based contrast agent: implications for imaging of deep tumors using optoacoustic tomography. *Mol. Imaging Biol.* 6:341–349.
37. Elghanian, R., J. J. Storhoff, …, C. A. Mirkin. 1997. Selective colorimetric detection of polynucleotides based on the distance-dependent optical properties of gold nanoparticles. *Science.* 277:1078–1081.
38. Jain, P. K., W. Huang, and M. A. El-Sayed. 2007. On the universal scaling behavior of the distance decay of plasmon coupling in metal nanoparticle pairs: a plasmon ruler equation. *Nano Lett.* 7:2080–2088.
39. Maye, M. M., D. Nykypanchuk, …, O. Gang. 2009. Stepwise surface encoding for high-throughput assembly of nanoclusters. *Nat. Mater.* 8:388–391.
40. Pace, C. N., F. Vajdos, …, T. Gray. 1995. How to measure and predict the molar absorption coefficient of a protein. *Protein Sci.* 4:2411–2423.
41. Sukumar, M., B. L. Doyle, …, A. H. Pekar. 2004. Opalescent appearance of an IgG1 antibody at high concentrations and its relationship to noncovalent association. *Pharm. Res.* 21:1087–1093.
42. Eck, D., C. A. Helm, …, K. A. Vaynberg. 2001. Plasmon resonance measurements of the adsorption and adsorption kinetics of a biopolymer onto gold nanocolloids. *Langmuir.* 17:957–960.
43. Kumar, S., J. Aaron, and K. Sokolov. 2008. Directional conjugation of antibodies to nanoparticles for synthesis of multiplexed optical contrast agents with both delivery and targeting moieties. *Nat. Protoc.* 3:314–320.
44. Pease, 3rd, L. F., J. T. Elliott, …, M. J. Tarlov. 2008. Determination of protein aggregation with differential mobility analysis: application to IgG antibody. *Biotechnol. Bioeng.* 101:1214–1222.
45. Bacher, G., W. W. Szymanski, …, G. Allmaier. 2001. Charge-reduced nano electrospray ionization combined with differential mobility analysis of peptides, proteins, glycoproteins, noncovalent protein complexes and viruses. *J. Mass Spectrom.* 36:1038–1052.
46. Buijs, J., J. W. T. Lichtenbelt, …, J. Lyklema. 1995. Adsorption of monoclonal Iggs and their $F(ab')_2$ fragments onto polymeric surfaces. *Colloid. Surface. B.* 5:11–23.
47. Zhou, C., J. M. Friedt, …, G. Borghs. 2004. Human immunoglobulin adsorption investigated by means of quartz crystal microbalance dissipation, atomic force microscopy, surface acoustic wave, and surface plasmon resonance techniques. *Langmuir.* 20:5870–5878.
48. Brewer, S. H., W. R. Glomm, …, S. Franzen. 2005. Probing BSA binding to citrate-coated gold nanoparticles and surfaces. *Langmuir.* 21:9303–9307.
49. Heinz, H., B. L. Farmer, …, R. R. Naik. 2009. Nature of molecular interactions of peptides with gold, palladium, and Pd-Au bimetal surfaces in aqueous solution. *J. Am. Chem. Soc.* 131:9704–9714.
50. Macdonald, I. D. G., and W. E. Smith. 1996. Orientation of cytochrome *c* adsorbed on a citrate-reduced silver colloid surface. *Langmuir.* 12:706–713.

51. Katz, E., and I. Willner. 2004. Integrated nanoparticle-biomolecule hybrid systems: synthesis, properties, and applications. *Angew. Chem. Int. Ed. Engl.* 43:6042–6108.

52. Aubin-Tam, M. E., and K. Hamad-Schifferli. 2008. Structure and function of nanoparticle-protein conjugates. *Biomed. Mater.* 3:034001.

53. Geoghegan, W. D. 1986. The adsorption of rabbit IgG to colloidal gold-molecular-orientation. *Acta Histochem.* 19:383.

54. Saluja, A., A. V. Badkar, …, D. S. Kalonia. 2007. Ultrasonic storage modulus as a novel parameter for analyzing protein-protein interactions in high protein concentration solutions: correlation with static and dynamic light scattering measurements. *Biophys. J.* 92:234–244.

55. Sahin, E., A. O. Grillo, …, C. J. Roberts. 2010. Comparative effects of pH and ionic strength on protein-protein interactions, unfolding, and aggregation for IgG1 antibodies. *J. Pharm. Sci.* 99:4830–4848.

56. Nishi, H., M. Miyajima, …, K. Fukui. 2010. Phase separation of an IgG1 antibody solution under a low ionic strength condition. *Pharm. Res.* 27:1348–1360.

57. Burckbuchler, V., G. Mekhloufi, …, F. Agnely. 2010. Rheological and syringeability properties of highly concentrated human polyclonal immunoglobulin solutions. *Eur. J. Pharm. Biopharm.* 76:351–356.

58. Neal, B. L., D. Asthagiri, and A. M. Lenhoff. 1998. Molecular origins of osmotic second virial coefficients of proteins. *Biophys. J.* 75:2469–2477.